Research Article | Vol. 8, No. 3 | 1 Mar 2017 | BIOMEDICAL OPTICS EXPRESS 1741
Biomedical Optics EXPRESS

Quantitative characteristics of sickle cell retinopathy in optical coherence tomography angiography

MINHAJ ALAM,[1] DAMBER THAPA,[1] JENNIFER I. LIM,[2] DINGCAI CAO,[2,3] AND XINCHENG YAO[1,2,4]

[1]*Department of Bioengineering, University of Illinois at Chicago, Chicago, IL 60607, USA*
[2]*Department of Ophthalmology and Visual Sciences, University of Illinois at Chicago, Chicago, IL 60612, USA*
[3]*dcao98@uic.edu*
[4]*xcy@uic.edu*

Abstract: Early detection is an essential step for effective intervention of sickle cell retinopathy (SCR). Emerging optical coherence tomography angiography (OCTA) provides excellent three-dimensional (3D) resolution to enable label-free, noninvasive visualization of retinal vascular structures, promising improved sensitivity in detecting SCR. However, quantitative analysis of SCR characteristics in OCTA images is yet to be established. In this study, we conducted comprehensive analysis of six OCTA parameters, including blood vessel tortuosity, vessel diameter, vessel perimeter index (VPI), area of foveal avascular zone (FAZ), contour irregularity of FAZ and parafoveal avascular density. Compared to traditional retinal thickness analysis, five of these six OCTA parameters show improved sensitivity for SCR detection than retinal thickness. It is observed that the most sensitive parameters were the contour irregularity of FAZ in the superficial layer and avascular density in temporal regions, while the area of FAZ, tortuosity and mean diameter of the vessel were moderately sensitive.

OCIS codes: (170.4470) Ophthalmology; (170.3880) Medical and biological imaging; (170.4500) Optical coherence tomography; (170.4580) Optical diagnostics for medicine; (330.4270) Vision system neurophysiology; (330.5380) Physiology; (330.4300) Vision system - noninvasive assessment.

References and links

1. K. L. Hassell, "Population estimates of sickle cell disease in the U.S," Am. J. Prev. Med. **38**(4 Suppl), S512–S521 (2010).
2. Sickcel Cell Guideline Panel, "Sickle Cell Disease: Screening, Diagnosis, Management, and Counseling in Newborns and Infants," AHCPR publication no. 93–0562 (Agency for Health Care Policy and Research, US Public Health Service, Rockville, MD: 1993).
3. M. F. Goldberg, "Classification and pathogenesis of proliferative sickle retinopathy," Am. J. Ophthalmol. **71**(3), 649–665 (1971).
4. J. I. Lim, "Ophthalmic manifestations of sickle cell disease: update of the latest findings," Curr. Opin. Ophthalmol. **23**(6), 533–536 (2012).
5. Q. V. Hoang, F. Y. Chau, M. Shahidi, and J. I. Lim, "Central macular splaying and outer retinal thinning in asymptomatic sickle cell patients by spectral-domain optical coherence tomography," Am. J. Ophthalmol. **151**(6), 990–994 (2011).
6. G. K. Asdourian, K. C. Nagpal, B. Busse, M. Goldbaum, D. Patriankos, M. F. Rabb, and M. F. Goldberg, "Macular and perimacular vascular remodelling sickling haemoglobinopathies," Br. J. Ophthalmol. **60**(6), 431–453 (1976).
7. W. Minvielle, V. Caillaux, S. Y. Cohen, F. Chasset, O. Zambrowski, A. Miere, and E. H. Souied, "Macular microangiopathy in sickle cell disease using optical coherence tomography angiography," Am. J. Ophthalmol. **164**, 137–144 (2016).
8. R. K. Wang, S. L. Jacques, Z. Ma, S. Hurst, S. R. Hanson, and A. Gruber, "Three dimensional optical angiography," Opt. Express **15**(7), 4083–4097 (2007).
9. E. Moult, W. Choi, N. K. Waheed, M. Adhi, B. Lee, C. D. Lu, V. Jayaraman, B. Potsaid, P. J. Rosenfeld, J. S. Duker, and J. G. Fujimoto, "Ultrahigh-speed swept-source OCT angiography in exudative AMD," Ophthalmic Surg. Lasers Imaging Retina **45**(6), 496–505 (2014).
10. T. S. Hwang, Y. Jia, S. S. Gao, S. T. Bailey, A. K. Lauer, C. J. Flaxel, D. J. Wilson, and D. Huang, "Optical coherence tomography angiography features of diabetic retinopathy," Retina **35**(11), 2371–2376 (2015).

#279784 https://doi.org/10.1364/BOE.8.001741
Journal © 2017 Received 1 Nov 2016; revised 10 Jan 2017; accepted 16 Jan 2017; published 23 Feb 2017

Biomedical Optics EXPRESS

11. Y. Jia, S. T. Bailey, T. S. Hwang, S. M. McClintic, S. S. Gao, M. E. Pennesi, C. J. Flaxel, A. K. Lauer, D. J. Wilson, J. Hornegger, J. G. Fujimoto, and D. Huang, "Quantitative optical coherence tomography angiography of vascular abnormalities in the living human eye," Proc. Natl. Acad. Sci. U.S.A. **112**(18), E2395–E2402 (2015).
12. Z. Chu, J. Lin, C. Gao, C. Xin, Q. Zhang, C. L. Chen, L. Roisman, G. Gregori, P. J. Rosenfeld, and R. K. Wang, "Quantitative assessment of the retinal microvasculature using optical coherence tomography angiography," J. Biomed. Opt. **21**(6), 066008 (2016).
13. Y. Jia, O. Tan, J. Tokayer, B. Potsaid, Y. Wang, J. J. Liu, M. F. Kraus, H. Subhash, J. G. Fujimoto, J. Hornegger, and D. Huang, "Split-spectrum amplitude-decorrelation angiography with optical coherence tomography," Opt. Express **20**(4), 4710–4725 (2012).
14. P. I. Condon and G. R. Serjeant, "Ocular findings of elderly cases of homozygous sickle-cell disease in Jamaica," Br. J. Ophthalmol. **60**(5), 361–364 (1976).
15. G. Goodman, L. Von Sallmann, and M. G. Holland, "Ocular manifestations of sickle-cell disease," AMA Arch. Opthalmol. **58**(5), 655–682 (1957).
16. E. W. Smith, C. L. Conley, "Clinical features of the genetic variants of sickle cell disease," Bulletin of the Johns Hopkins Hospital **94.6**(1954).
17. H. Azegrouz, "Thickness dependent tortuosity estimation for retinal blood vessels," Engineering in Medicine and Biology Society, 2006. EMBS'06. 28th Annual International Conference of the IEEE (2006).
18. S. G. Gadde, N. Anegondi, D. Bhanushali, L. Chidambara, N. K. Yadav, A. Khurana, and A. Sinha Roy, "Quantification of vessel density in retinal optical coherence tomography angiography images using local fractal dimension," Invest. Ophthalmol. Vis. Sci. **57**(1), 246–252 (2016).
19. T. Y. Kong and A. Rosenfeld, "Topological Algorithms for Digital Image Processing," Elsevier Science (1996).
20. L. Lam, S.-W. Lee, and C. Y. Suen, "Thinning methodologies-a comprehensive survey," IEEE Trans. Pattern Anal. Mach. Intell. **14**(9), 869 (1992).
21. D. Bracher, "Changes in peripapillary tortuosity of the central retinal arteries in newborns. A phenomenon whose underlying mechanisms need clarification," Graefes Arch. Clin. Exp. Ophthalmol. **218**(4), 211–217 (1982).
22. L. Zhou, M. S. Rzeszotarski, L. J. Singerman, and J. M. Chokreff, "The detection and quantification of retinopathy using digital angiograms," IEEE Trans. Med. Imaging **13**(4), 619–626 (1994).
23. M. H. Goldbaum, W. E. Hart, B. L. Cote, and P. V. Raphaelian, "Automated measures of retinal blood vessel tortuosity," Invest. Ophthalmol. Vis. Sci. **35**, 2089 (1994).
24. O. Smedby, N. Högman, S. Nilsson, U. Erikson, A. G. Olsson, and G. Walldius, "Two-dimensional tortuosity of the superficial femoral artery in early atherosclerosis," J. Vasc. Res. **30**(4), 181–191 (1993).
25. W. E. Hart, M. Goldbaum, B. Côté, P. Kube, and M. R. Nelson, "Measurement and classification of retinal vascular tortuosity," Int. J. Med. Inform. **53**(2-3), 239–252 (1999).
26. T. F. Chan, B. Y. Sandberg, and L. A. Vese, "Active contours without edges for vector-valued images," J. Vis. Commun. Image Represent. **11**(2), 130–141 (2000).
27. T. F. Chan and L. A. Vese, "Active contours without edges," IEEE Trans. Image Process. **10**(2), 266–277 (2001).
28. S. K. Alam, E. J. Feleppa, M. Rondeau, A. Kalisz, and B. S. Garra, "Ultrasonic multi-feature analysis procedure for computer-aided diagnosis of solid breast lesions," Ultrason. Imaging **33**(1), 17–38 (2011).
29. B. Aliahmad, D. K. Kumar, M. G. Sarossy, and R. Jain, "Relationship between diabetes and grayscale fractal dimensions of retinal vasculature in the Indian population," BMC Ophthalmol. **14**(1), 152 (2014).
30. R. Broe, M. L. Rasmussen, U. Frydkjaer-Olsen, B. S. Olsen, H. B. Mortensen, T. Peto, and J. Grauslund, "Retinal vascular fractals predict long-term microvascular complications in type 1 diabetes mellitus: the Danish Cohort of Pediatric Diabetes 1987 (DCPD1987)," Diabetologia **57**(10), 2215–2221 (2014).
31. J. W. Yau and R. Kawasaki, "Retinal fractal dimension is increased in persons with diabetes but not impaired glucose metabolism: the Australian Diabetes, Obesity and Lifestyle (AusDiab) study," Diabetologia **53**(9), 2042–2045 (2010).
32. O. S. Al-Kadi and D. Watson, "Texture analysis of aggressive and nonaggressive lung tumor CE CT images," IEEE Trans. Biomed. Eng. **55**(7), 1822–1830 (2008).
33. H. Taud and J.-F. Parrot, "Measurement of DEM roughness using the local fractal dimension," G'eomorphologie **11**(4), 327–338 (2005).
34. A. Zhang, Q. Zhang, and R. K. Wang, "Minimizing projection artifacts for accurate presentation of choroidal neovascularization in OCT micro-angiography," Biomed. Opt. Express **6**(10), 4130–4143 (2015).
35. Q. Zhang, "Projection Artifact Removal Improves Visualization and Quantitation of Macular Neovascularization Imaged by Optical Coherence Tomography Angiography " Ophthalmology Retina (Posted 2 November 2016, In press).

1. Introduction

Sickle Cell Disease (SCD) is an inherited red blood cell disorder that affects 90,000 – 100,000 Americans [1], making it one of the most prevalent genetic disorders in the United States [2]. Red blood cells with normal hemoglobin have a disc shape and this round shape allows the cells to be flexible so that they can move through not only large blood vessels but also small capillaries to deliver oxygen. In SCD, however, red blood cells deform into a C-shaped farm

Biomedical Optics EXPRESS

tool called a "sickle". When sickle cells travel through small blood vessels, they can get stuck and occlude blood flow and thus prevent oxygen from reaching vital organs. Consequently, patients with SCD suffer from microvascular occlusions in various parts of their body, including the retina. Sickle cell retinopathy (SCR) is one of the major ocular manifestations of SCD. The underlying systemic and ocular manifestations of SCD are a result of vaso-occlusive ischemia due to the blocking of blood vessels by sickle-shaped erythrocytes.

SCR typically involves peripheral retinal vessels. At this time, the clinical staging system is of limited value in predicting progression of SCR. Further, standard fundus-based clinical examination typically shows normal to minimal findings in the macular area in sickle cell patients [3]. Although patients are asymptomatic, many adult sickle cell patients do harbor findings of SCR that precede the clinical detection of a foveal depression sign [4], such as macular thinning measured by optical coherence tomography (OCT) [5] or vascular abnormalities in the macular region based on fluorescein angiography (FA) [6]. However, the existing techniques are limited in detecting subclinical signs of SCR. For instance, FA requires dye injection and cannot detect abnormalities in ~50% of eyes in sickle cell patients, compared with recently emerged OCT Angiography (OCTA) [7]. New technique is desirable for detecting subclinical sign of SCR.

OCTA has been used for quantitative assessment of retinal vascular structures [8–12]. OCTA allows visualization of multiple retinal layers with high resolution and therefore is more sensitive than traditional FA in detecting SCR [7]. Thus, OCTA may be able to further the classification of SCR by including data with prognostic value. OCTA is currently available commercially for clinical use. However, quantitative analysis of SCR characteristics in OCTA images is yet to be established. In this study, we conducted comparative analysis of six OCTA parameters, including blood vessel tortuosity, vessel diameter, vessel perimeter index (VPI), area of foveal avascular zone (FAZ), contour irregularity of FAZ and parafoveal avascular density of control and SCR groups. The goal was to assess how the parameters correlated with retinal thickness and how sensitive the parameters could detect SCR, and thus to establish a metric for quantitative OCTA assessment of SCR.

2. Materials and methods

2.1 Data acquisition

This study was approved by the Institutional Review Board of the University of Illinois at Chicago and was in compliance with the ethical standards stated in the Declaration of Helsinki. The SCD patients were recruited from University of Illinois at Chicago (UIC) Retinal Clinic. The majority of patients (N = 14, 78%) had Stage II of retinopathy with the remaining as Stage III (N = 4, 22%). The quantitative study was based on OCTA images of 18 SCD patients (7 males and 11 females; 18 African Americans) and 13 control subjects (12 males, 1 female, 3 African Americans). The mean age was 40 years (range 24 to 64) for the patients and 37 years (range 25 to 71) for the control. OCTA images of both eyes (OS and OD) were analyzed in this study, so the database consisted of 36 SCR eyes and 26 control eyes. The subjects of the control group were chosen based on their previous ocular history, absence of any systemic diseases, or any visual symptoms; a normal- appearing retina on clinical examination; and a normal reflectance OCT of the macula.

SD-OCT data was acquired using an ANGIOVUE SD-OCT angiography system (OPTOVUE, Fremont, CA, USA), with a 70-KHz A-scan rate. OCTA images were constructed using split-spectrum amplitude-decorrelation angiography (SSADA) algorithm with integrated motion correction algorithm [13]. The axial resolution is ~5 μm while lateral resolution is ~15 μm. The scanning protocol in this system provided a field of view (FOV) of 3 mm × 3 mm, 6 mm × 6 mm or 8 mm × 8 mm. For our calculation, we used only 3 mm × 3 mm portions from the OCTA images. OCT angiography images were exported using the software ReVue (Optovue, Fremont, CA). The ReVue was used to segment superficial and

Biomedical Optics EXPRESS

deep inner retinal vascular plexuses. It was also used to measure the retinal thickness from the OCT B-scans, the thickness was measured from the outermost layer of fovea to the retinal pigment epithelium (RPE) layer. Custom-developed MATLAB (R2015b, MathWorks, Inc.) procedures with graphical user interface (GUI) were used for further image analysis and quantitative comparison.

2.2 Quantitative parameters for OCTA analysis

Six OCTA parameters, including blood vessel tortuosity, vessel diameter, VPI, area of FAZ, contour irregularity of FAZ and parafoveal avascular density, were used to analyze and quantify the OCTA images from SCD patients and compare the patient data with control subjects using Student t-tests. Effect sizes (Cohen's d) were also calculated to quantify the difference in the outcome between the groups normalized by the pooled standard deviations. Pearson correlations between retinal thickness and the OCTA parameters were computed separately for the controls and SCD patients. Finally, canonical discriminant analysis was conducted to assess which measurements (retinal thickness, OCTA parameters) were most sensitive to differentiate SCD patients vs. controls. For the discriminant analysis, the variables with small canonical loadings (correlations between the observed variables and the discriminant function) were sequentially removed until all remaining variables had canonical loadings > 0.3 (a critical loading value for a variable considered to be important).

The rationale of each of these six OCTA parameters is briefly summarized in the following sessions.

2.2.1 Blood vessel tortuosity

Retinal blood vessels in SCD patients are known to be more tortuous than those in normal subjects [14–16], due to sickle cell anemia. Therefore, quantitative analysis of blood vessel tortuosity can be valuable. In this study, quantitative analysis of the tortuosity is conducted for large blood vessel branches in the superficial layer. As the sickle cells affects the retinal vasculature, the tortuosity is visually prominent in large vessels and they have statistically more reliable tortuosity measurement index [17].The first step is to reconstruct *en-face* OCTA image of the superficial layer of retina (Fig. 1(a)). The second step is to segment the large blood vessels using global thresholding [12], morphological functions (Fig. 1(b)) and fractal dimension classification [18]. This binary vasculature map was then skeletonized. The skeletonization process removes pixels on the boundaries of vessels but does not allow objects to break apart [19, 20]. The remaining pixels make up the image skeleton. After this, each branch of the blood capillaries was identified with two endpoints (points A and B in Fig. 1(c)) so that the geodesic and Euclidian distances for each branch could be calculated. The tortuosity of a single branch is defined by the distance metric [21–25] which is the ratio of geodesic distance and Euclidean distance between the two endpoints. For two points A(x1, y1) and B(x2, y2) in a two dimensional plane as shown in Fig. 1, Euclidean distance is calculated using the following equation [25],

$$Euclidean\,distance = \sqrt{(x_1 - x_2)^2 + (y_1 - y_2)^2}. \quad (1)$$

If we define each of the segmented branches with [x(t),y(t)] on the interval [t_0, t_1], the geodesic distance between the endpoints i.e. A and B can be calculated with the following equation [25],

$$Geodesic\,distance = \int_{t_0}^{t_1} \sqrt{\left(\frac{dx(t)}{dt}\right)^2 + \left(\frac{dy(t)}{dt}\right)^2}\, dt. \quad (2)$$

The tortuosity of each branch of blood vessels was calculated and the average tortuosity of the image was measured [25],

Biomedical Optics EXPRESS

$$Tortuosity = \frac{1}{n}\sum_{i=1}^{n}\left(\frac{Geodesic\ distance\ between\ two\ endpoints\ of\ a\ vessel\ branch\ i}{Euclidean\ distance\ between\ two\ endpoints\ of\ a\ vessel\ branch\ i}\right). \quad (3)$$

where *i* is the ith branch and n is the number of branch.

2.2.2 Mean diameter of blood vessel

As the sickle cells affect the blood flow inside the vessels and thus cause structural change in the vasculature, the mean diameter of blood vessels is an important parameter to analyze in OCTA images. Large blood vessels from superficial *en-face* OCTA image were measured to quantify this parameter. The large vessel area was calculated from the vessel map (Fig. 1(b)) and length was calculated from the skeleton map (Fig. 1(c)). Mean vessel diameter was then calculated as the ratio of vessel area and length using the following equation [12],

$$Mean\ vessel\ width = \frac{\sum_{i=1,j=1}^{n} B(i,j)}{\sum_{i=1,j=1}^{n} S(i,j)}. \quad (4)$$

where B (i,j) represents the pixels occupied by the vessels and S (i,j) represents the pixels occupied by the vessel skeleton (i, j represent the row and column positions of each pixel of the image). With this parameter, localized vascular dilation would be easily identified and it could serve as a marker for vascular abnormalities.

2.2.3 Vessel perimeter index (VPI)

Large blood vessels in the *en-face* OCTA image were used to measure this parameter. From the binary vasculature map, a vessel perimeter map (Fig. 3(a)) was obtained by detecting the edge of vessels and deleting the pixels that were not close to the edge of the vessels. The VPI was calculated as the ratio of perimeter pixel area and total image area using the following equation [12],

$$Vessel\ perimeter\ index = \frac{\sum_{i=1,j=1}^{n} P(i,j)}{\sum_{i=1,j=1}^{n} I(i,j)}. \quad (5)$$

where P (i,j) represents the pixels within the vessel perimeters (white pixels on Fig. 3(a)) and I (i,j) represents all the pixels in the vessel perimeter map. This parameter is a good marker of overall change of vessel length in OCTA images.

2.2.4 Area of FAZ

Since the SC disease directly affects the vessel texture with tortuosity and dilation, it is also interesting to compare the change in foveal avascular area for control subjects and SCD patients. The FAZ contour was semi-automatically demarcated and the FAZ was segmented from the OCTA images (Fig. 4(a), 4(d)) using an active contour model [26, 27], where the seed point was manually placed at the center of the fovea. The pixel size of the OCTA image is a known parameter and from this information, the area of the avascular region was calculated using the following equation [12],

$$FAZ = (Area\ of\ single\ pixel\ (in\ \mu m^2)) \times \sum_{i=1,j=1}^{n} A(i,j). \quad (6)$$

where A (i,j) represents the pixels occupied by the segmented avascular region.

Biomedical Optics EXPRESS

2.2.5 Contour irregularity of FAZ

A contour irregularity parameter can be used to express border irregularity and is also an excellent descriptor of spiculation, i.e, spiked nature of the contour [28]. We illustrate the effects of increasing border roughness using contours of avascular area (Fig. 4(c), 4(f)). The bigger the value of contour irregularity, the more irregular and spiked the contour of the avascular region is. Contour irregularity parameter was calculated with the following equation [28],

$$Contour\,irregularity = \frac{\sum_{i=1,j=1}^{n} O(i,j)}{\sum_{i=1,j=1}^{n} R(i,j)}. \tag{7}$$

where O (i,j) represents the pixels occupied by the FAZ contour and R (i,j) represents the pixels occupied by the perimeter of the reference circle.

The contour of the original avascular region was measured; a circle of the same area as the avascular region was used as a reference.

2.2.6 Density of parafoveal avascular region

In order to quantify the density of parafoveal avascular region, fractal dimension (FD) analysis of both the superficial and deep layers were conducted [18]. FD has been considered as a potential biomarker for retina-based disease detection [29–31]. Fractal is non-Euclidean structures that show self-similarity at different scales. The FD of a structure provides a measure of its texture complexity [32]. The retinal blood vessels and capillaries are complex and rarely have an exact Euclidean shape. Therefore, they can be precisely described by fractal analysis. Many retinal diseases such as SC disease involve vessel abnormalities, including drop out zones in between vascular structures. This requires detailed analysis of the retinal vasculature to understand their role in disease pathophysiology. In our case, local fractal dimension (LFD) analysis which identifies local variations in the vascular network was calculated from the OCTA images by using a moving window of size $(2w+1)\times(2w+1)$ using the following equation [33],

$$q(i,j) = LFD[\mathrm{p}(\mathrm{i}+\mathrm{k},\mathrm{j}+\mathrm{k});\ -\mathrm{w} < k < w]. \tag{8}$$

where $p(i,j)$ is the intensity OCTA image, $q(i,j)$ is the fractal dimension of the intensity image and (i,j) corresponds to the location of each pixel in the image. Local FD was calculated using window sizes (in pixels) of 3 × 3, 5 × 5, 7 × 7, 9 × 9 and 11 × 11 (w = 1,2,3,4.5).

The FD varies across the image; it is higher in larger vessels compared to that in smaller vessel or non-vascular region [18]. Therefore, the LFD was normalized and plotted as a contour plot (Fig. 5(a), 5(b)). The normalized LFD with a value close to 1 indicates large vessels and a value close to 0 indicates non-vessel regions, so the regions were classified as follows: the blood vessels and capillaries lie between a value of 0.7 and 1; the nonvascular regions lie between a value of 0.0 and 0.3 and the smaller gaps between vessels lie between a value of 0.3 and 0.7, we define this area as grey zone. The density calculation is expressed in percentage by taking the ratio of the total pixels with corresponding FD values (0 to 0.3 for non-vascular region, 0.7 to 1 for vessel and 0.3 to 0.7 for grey zone) to the total pixels in the analyzed window [18]. Here, vessel densities were calculated in three circular parafoveal regions of diameter 1 mm, 2 mm and 3 mm as shown in Fig. 5(a) and four parafoveal sectors, namely, nasal (N), superior (S), temporal (T), and inferior (I) of a circular zone of diameter 3 mm as shown in Fig. 5(b).

Biomedical Optics EXPRESS

3. Results

In Section 3.1 we report the OCTA measurements and their respective variation with SCD. In Section 3.2, we provide comparative information of retinal thickness and discriminant analysis. Among 36 SCR OCTA images in total, 1 OD and 3 OS OCTA images were excluded due to severe image distortions.

3.1. OCTA parameters

3.1.1 Blood vessel tortuosity

Figure 1 illustrates representative OCTA image (Fig. 1(a)), segmented blood vessel map (Fig. 1(b)) and skeletonized blood vessel map (Fig. 1(c)). The retinal vasculature in SCD patients becomes more complex as the vessels become more tortuous and twisted. As shown in Fig. 1(d), SCD eyes had much higher tortuosity than the control eyes (48.07% vs. 31.52%, $p < 0.001$, Cohen's $d = 3.69$). On average, a tortuosity increase of 16.56% was observed in SCD patients compared to control subjects.

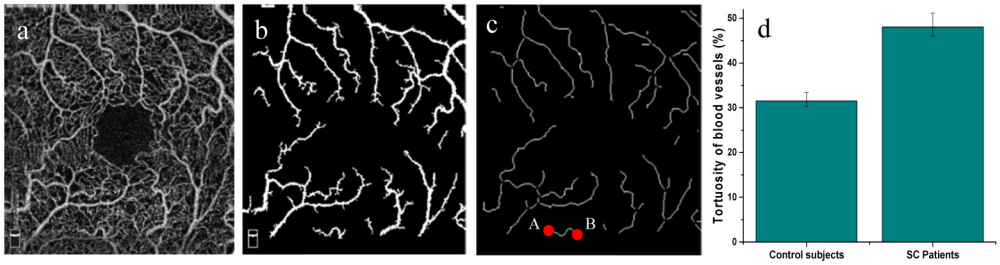

Fig. 1. Measuring tortuosity of OCTA images. (a) OCTA raw image, (b) Segmented large blood vessel map, (c) Skeletonized blood vessels branches with identified endpoints (for a random vessel branch, A and B endpoints are shown with red dots), (d) Comparison of tortuosity in control and SC patients (error bars are standard deviations).

3.1.2 Mean diameter of blood vessel

Figure 2 illustrates the mean diameters of large blood vessels of superficial OCTA images. It was observed that the averaged diameter of blood vessels of control subjects and SCD patients were 23.65 μm and 30.60 μm, respectively. The mean diameter increased about 29.4% in SCD patients, reflecting a significant dilation in the large blood vessels of SCD patients ($p<0.01$, Cohen's $d = 3.18$).

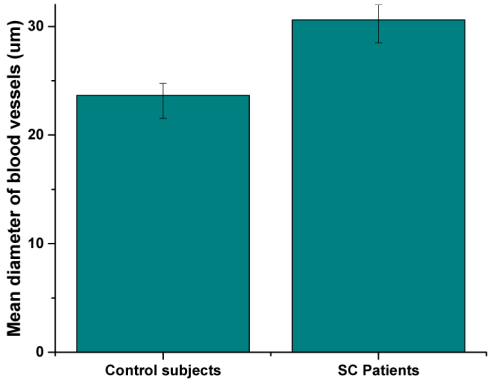

Fig. 2. Comparison of mean diameter of blood vessels in control and SC patients (superficial layer).

Biomedical Optics EXPRESS

3.1.3 Vessel perimeter index (VPI)

Figure 3(a) illustrates the binary vessel perimeter map obtained from the superficial raw OCTA image (Fig. 1(a)). VPI provides a good estimation of the change in vessel length for SCD patients. As shown in Fig. 3(b), the VPI in control subjects is 10.8% and it is 8.31% in SCD patients, so there is a decrease of 2.49% in VPI for SCD patients ($p<0.05$, Cohen's d = 2.41).

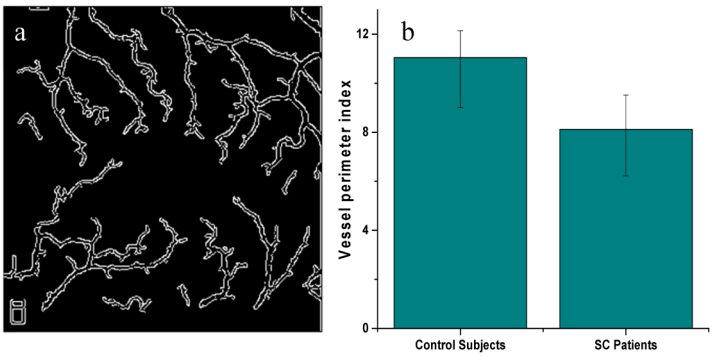

Fig. 3. (a) Vessel perimeter map, (b) Comparison of VPI in control and SCD patients (superficial layer).

3.1.4 Area of FAZ

Figure 4(a) and 4(d) illustrates the demarcation of FAZ in raw OCTA images, in control and SCD patients respectively with the binary FAZ segmentation (Fig. 4(b) and 4(e)) and contour map (Fig. 4(c) and 4(f)). It was observed that the average area of avascular region also increases in SCD patients (52% in deep and 53% in superficial layer). This shows that, for SCD patients FAZ increases, which is possibly a result of rapid drop out of retinal vessels near foveal area ($p<0.001$, Cohen's d = 4.15). The comparison is illustrated in Fig. 4(g).

3.1.5 Contour irregularity of FAZ

From the segmented FAZ (Fig. 4(b), 4(e)) we also measured the contour of the region (Fig. 4(c), 4(f)). As there are complex vascular structure and vessel abnormalities, the contour becomes more irregular in SCD patients rather than a smooth shape in control subjects. The contour irregularity index for control subjects are 1.10 and 1.11 for deep and superficial layers respectively.

Biomedical Optics EXPRESS

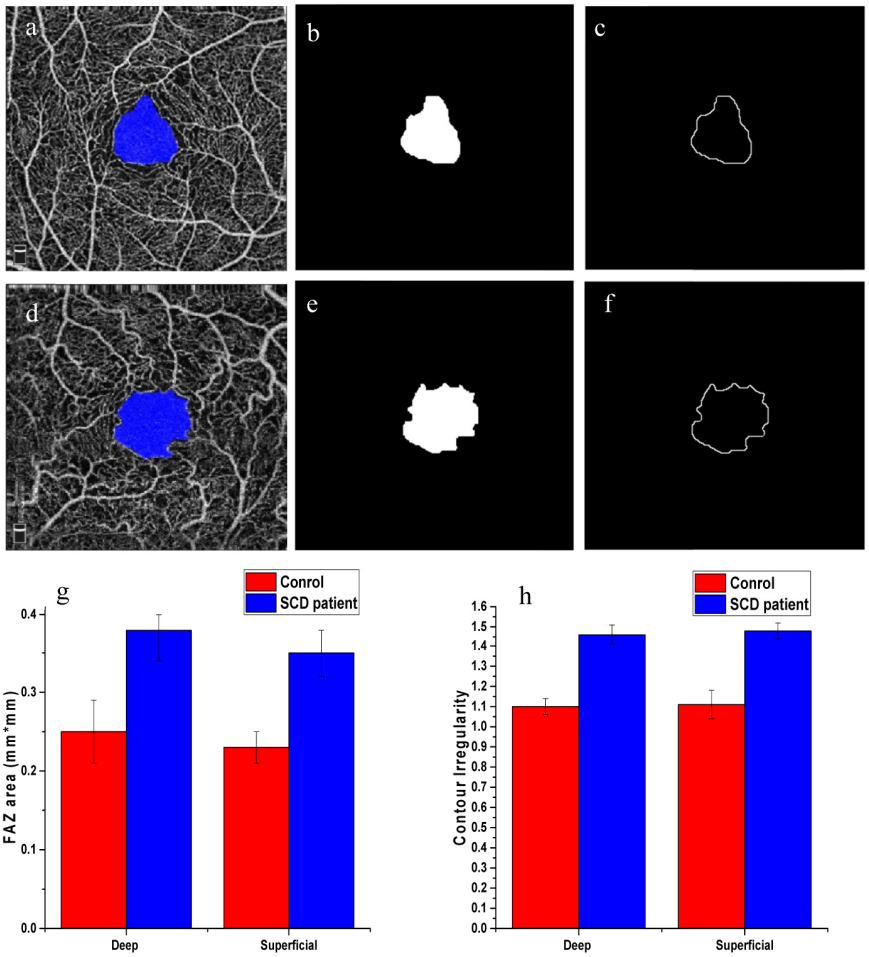

Fig. 4. (a) OCTA image with demarcation for normal eye, (b) Segmented Avascular region for normal eye (c) FAZ contour for normal eye, (d) OCTA image with demarcation for diseased eye, (e) Segmented avascular region for diseased eye, (f) FAZ contour for diseased eye, (g) Comparison of area of FAZ in control and SCD patients for deep and superficial layers, (h) Comparison of area of FAZ in control and SCD patients for deep and superficial layers.

Our results show that the contour of FAZ from control subjects has 10-11% deviation from an ideal circular contour whereas the contour from the SCD patients has around 46-47% deviation (comparison shown in Fig. 4(h)). The irregularity and spiculation increase by almost 36% in case of SCD patients for both deep and superficial layers. This clearly indicates the feasibility of this parameter (contour irregularity) as a biomarker of SC disease (p<0.001, Cohen's d = 4.52).

3.1.6 Density of parafoveal avascular region

Figure 5 illustrates the contour maps with normalized values of local fractal dimension corresponding to OCTA raw images; it also shows the different regions or zones of the image where FD analysis was conducted (Fig. 5(a), 5(b)). A detailed vasculature density analysis was conducted with the OCTA database. SC disease can lead to vessel drop out zones in the vascular structure of retina, so we measured the density of non-vascular region, vessels, intermediate gaps (grey zones) and compared the changes in density in definite zones. The density comparison was done in three circular parafoveal regions of diameter 1 mm, 2 mm

Biomedical Optics EXPRESS

and 3 mm (Fig. 5(a)) and four parafoveal sectors, namely, nasal (N), superior (S), temporal (T), and inferior (I) of a circular zone of diameter 3 mm (Fig. 5(b)). The avascular region increased significantly in SCD patients (p<0.01, Cohen's d = 3.24), the vessel density and grey zone density decreased to compensate for the increase of non-vascular regions.

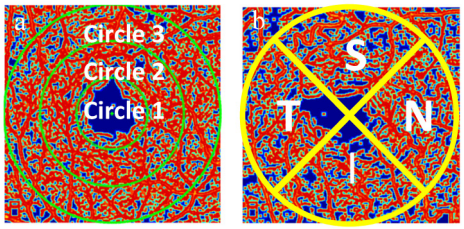

Fig. 5. Contour maps created with normalized values of local fractal dimension. (a) Circular zones of diameter 1, 2 and 3mm, (b) Nasal, Superior, Temporal and Inferior regions. FD analysis was conducted on the different regions specified in a and b.

Table 1. Vascular density changes in different zones

Vascular density changes in different zones						
	Superficial Layer			Deep Layer		
	Avascular region	Grey Zone	Vessel density	Avascular region	Grey Zone	Vessel density
Circle 1	18.37%↑*	5.72%↓*	12.65%↓*	5.82%↑*	2.64%↓*	3.18%↓*
Circle 2	12.70%↑**	4.43%↓**	8.27%↓**	9.66%↑**	3.53%↓**	6.12%↓**
Circle 3	13.25%↑**	4.83%↓**	8.42%↓**	13.85%↑**	4.21%↓**	9.64%↓**
N	12.60%↑**	4.25%↓**	8.35%↓**	14.40%↑**	4.53%↓**	9.87%↓**
S	12.55%↑*	2.98%↓*	9.57%↓*	14.45%↑*	5.57%↓*	8.88%↓*
T	14.34%↑***	3.45%↓***	10.92%↓***	17.26%↑***	6.8%↓***	10.46%↓***
I	12.35%↑*	2.57%↓*	9.78%↓*	13.44%↑*	4.77%↓*	8.67%↓*

A summary of the vasculature density analysis of FD contour map is shown in the Table 1 and illustrated in Fig. 6 where we can observe the increase of avascular region density for each specific zone and the decrease of grey zone and large vessel densities. For each section in Table 1 the significance of the t-test is marked as: * for $p < 0.05$; ** $p < 0.01$; *** $p < 0.001$.

Biomedical Optics EXPRESS

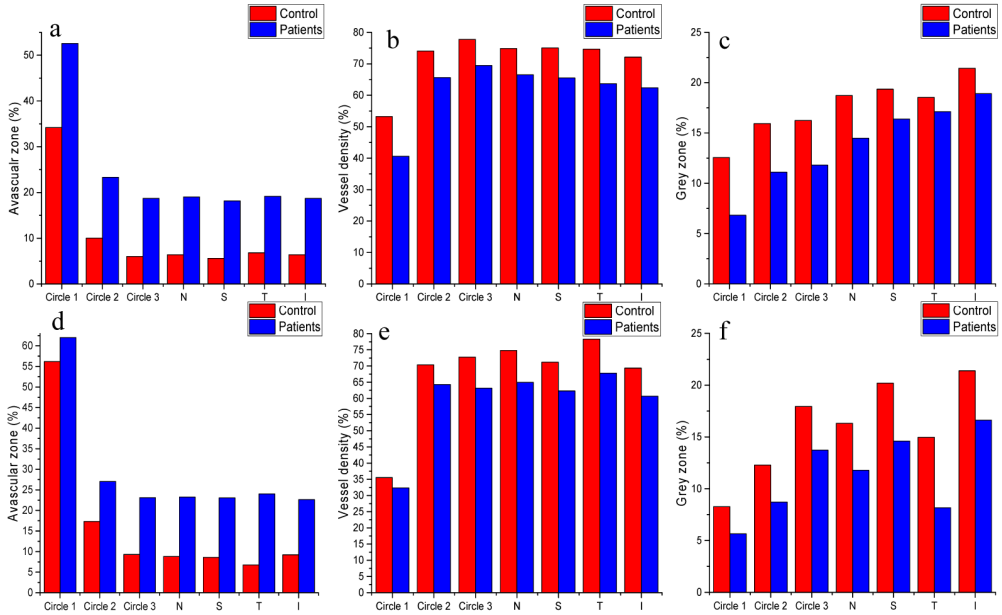

Fig. 6. Comparison of vascular density in different sections of the OCTA image in control and patient eyes. Control eye: (a) Avascular region density, (b) Vessel density, (c) Grey zone density; Patient eye: (d) Avascular region density, (e) Vessel density, (f) Grey zone density.

We have also summarized the results for the first five parameters in Table 2. It illustrates the effect of SCD for the parameters and their sensitivity to it. By observing the P values from the t-test results we get the indication whether the change due to SCD is significant or not.

Table 2. Quantitative comparison of parameters

Parameters	Average Tortuosity	Average Diameter of Blood Vessels (μm)	Vessel Perimeter Index	Area of FAZ (mm^2)		FAZ Contour Irregularity	
Retinal Layers	Superficial	Superficial	Superficial	Deep	Superficial	Deep	Superficial
Control	31.52	23.65	10.80	0.25	0.23	1.10	1.11
Patients	48.07	30.60	8.31	0.38	0.35	1.46	1.47
Change in parameters	16.56%↑	29.40%↑	2.49%↓	52%↑	53%↑	36%↑	36%↑
P value	<0.001	<0.01	<0.05	<0.001		<0.001	
Cohen's d	3.69	3.18	2.41	4.15		4.52	

3.2. Retinal thickness and discriminant analysis

Retinal thickness was significantly lower in SCD patients than controls (193.61 ± 5.31 um vs. 217.67 ± 6.44 um, $p < 0.001$, Cohen's d = 3.68). None of the OCTA parameters were significantly correlated with the retinal thickness either in controls or SCD patients except for the area of FAZ in Circle 1 of the superficial layer in SCD patients ($r = –0.73$, $p < 0.001$). This correlation analysis suggested that OCTA parameters provided additional information of retinal health than retinal thickness.

Biomedical Optics EXPRESS

Canonical discriminant analysis using retinal thickness and the OCTA parameters indicated most of the OCTA parameters had higher canonical loadings than retinal thickness. The most sensitive OCTA parameters with canonical loadings > 0.3 included: 1) contour irregularity of FAZ in superficial layer, 2) avascular area of Circle 2 in superficial layer, 3) avascular area of the temporal region in superficial layer, and 4) avascular area of the inferior region in deep layer. These four variables could individually or jointly differentiate the SCD patients vs. controls with 100% correct rate.

4. Discussions

Six OCTA parameters, i.e., blood vessel tortuosity, diameter, VPI, area of FAZ, contour irregularity of FAZ and parafoveal avascular density were developed for quantitative assessment of OCTA images. 36 SCR and 26 normal OCTA images were used for comparative analysis. Among the 36 SCR OCTA images, 1 OD and 3 OS OCTA images were excluded due to severe image distortions. Pathological change of the retina, eye motion and enface OCTA projection artifacts were the main reasons behind the distortion. ReVue software utilizes SSADA algorithm for OCTA construction, with integrated motion correction algorithm. Potential incorporation of removal algorithm of projection artifacts [34, 35] may further improve the OCTA image quality.

A Pearson correlation analysis was conducted to test the relationship between traditional retinal thickness measurement and each of these six OCTA parameters. The analysis revealed that most of OCTA parameters are not significantly correlated with the retinal thickness except for the area of FAZ in Circle 1 (1 mm diameter or 0.5 mm radius from the center) of the superficial layer. This suggests that the OCTA may provide additional information on disease associated vasculature change than retinal thickness only information from traditional OCT. Morphological distortion of retinal blood vessels in SCD patients occurs due to sickle cell anemia [14–16]. Quantitative analysis of blood vessel tortuosity revealed 19.07% tortuosity increment in SCD group, compared to that in control group. A 29.40% increment of blood vessel diameter was observed in SCD group. A 2.49% decrease was observed for the VPI of the SCD group, which is consistent to the observed increment of blood vessel diameter. FAZ was consistently enlarged and contour irregularity was increased in SCD patients. The FAZ contour irregularity is closely related to tortuosity increase which makes the retinal vessels more irregular and spiked in shape. In contrary, retinal blood vessel densities in both superficial and deep layers were decreased in SCD retinas, compared to normal ones. It is known that proliferative SCD affects the peripheral retinal vasculature, and its manifestations include capillary dropout, arteriolar–venular anastomoses, development of retinal neovascularization and pigmentary changes. Our quantitative analysis of retinal vasculature with FD analysis confirms this effect of SCD on retinal vessels.

Another important aspect of this study was to test the sensitivity of each OCTA parameter for detecting SCR. The canonical discriminant analysis showed that OCTA parameters were more sensitive than retinal thickness and the most sensitive OCTA parameter was contour irregularity of FAZ in superficial layer, avascular density in circle 2 of superficial layer, avascular density in temporal region in superficial layer and avascular density in the inferior region in deep layer. These variables could correctly differentiate the SCD patients from the control subjects. According to the mean calculation of the parameter (supported by t-test and Cohen's d index), it was consistently observed that the most sensitive parameter was the area of FAZ (about 52-53% change in SCD patients) and contour irregularity (both superficial and deep layers) (about 36% change) (Table 2). Tortuosity, mean diameter of the vessels and avascular density in temporal regions are moderately sensitive in SCD patients (about 14-29% change). It can be seen that the contour irregularity in superficial layer and avascular density in temporal regions are the most sensitive parameters according to both discriminant analysis and t-test results obtained.

Biomedical Optics EXPRESS

5. Conclusions

Six parameters have been used for quantitative assessment of OCTA images. Comparative analysis of control and SCD groups reveals statistically significant differences for all of these six parameters. It is observed that the most sensitive parameters were the contour irregularity in superficial layer and avascular density in temporal regions while the area of FAZ, tortuosity and mean diameter of the vessel were moderately sensitive. It is confirmed that the parafoveal non-vascular region density increases as there are vessel drop outs due to SCD. As the non-vascular region increases, the grey zone and vessel density decreases. The study establishes use of the parameters as bio-marker for potential SCR diagnoses and provides a metric for quantifying changes in retinal vasculature in SCD patients.

Funding

This research was supported in part by NIH grants R01 EY023522, R01 EY024628, P30 EY001792; by NSF grant CBET-1055889; by Richard and Loan Hill endowment; by unrestricted grant from Research to Prevent Blindness; by Marion H. Schenck Chair endowment.

Acknowledgment

The authors thank Mr. Mark Janowicz for his help on OCTA data acquisition.